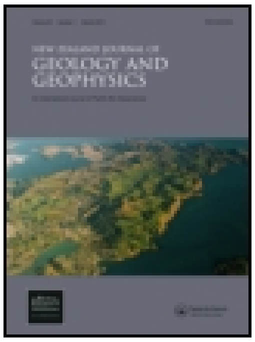

New Zealand Journal of Geology and Geophysics

ISSN: 0028-8306 (Print) 1175-8791 (Online) Journal homepage: http://www.tandfonline.com/loi/tnzg20

Geophysical imaging of disrupted coastal dune stratigraphy and possible mechanisms, Haast, South Westland, New Zealand

DC Nobes, HM Jol & B Duffy

NEW ZEALAND JOURNAL OF GEOLOGY AND GEOPHYSICS, 2016
http://dx.doi.org/10.1080/00288306.2016.1168455

RESEARCH ARTICLE

Geophysical imaging of disrupted coastal dune stratigraphy and possible mechanisms, Haast, South Westland, New Zealand

DC Nobes[a,b*], HM Jol[c] and B Duffy[b*,d]

[a]School of Nuclear Engineering and Geophysics, East China University of Technology, Economic Development Area, Nanchang, Jiangxi, China; [b]Department of Geological Sciences, University of Canterbury, Christchurch, New Zealand; [c]Department of Geography and Anthropology, University of Wisconsin – Eau Claire, Wisconsin, USA; [d]School of Earth Sciences, The University of Melbourne, Parkville, Australia

ABSTRACT
Geophysical imaging of coastal dune stratigraphy near Haast, South Westland, provides insight into coseismic dune modification on a seismically active coastline. Complementary ground-penetrating radar and electrical imaging responses reveal low-angle features that apparently truncate and offset dune bedding. Complex attribute analysis of the GPR profiles is consistent with truncated bedding. One feature is near-coastal and separates post-seismic dunes that have been attributed to the 1717 Alpine Fault and 1826 Fiordland earthquakes. Another is inland, coincident with an incised stream channel. Superficially, the truncations might be interpreted as erosional features caused by large storms; however, the truncating features penetrate and appear to disrupt the wave base. We therefore suggest the near-coastal truncation is either a translational feature, such as a slide, or more likely an erosional record of a tsunami generated by the 1826 Fiordland earthquake. The inland feature records a previous event, the cause of which needs further investigation.

ARTICLE HISTORY
Received 12 May 2015
Accepted 1 March 2016

KEYWORDS
Coastal dune; electrical imaging; ground penetrating radar; retreat scarp; South Westland; tsunami

Introduction

Tectonic forces are major drivers of landscape evolution and of range-front and coastal sedimentation in New Zealand and elsewhere, generating secondary fault ruptures, landslides, and tsunamis (e.g. Goff & McFadgen 2002; Wells & Goff 2006, 2007; Quigley et al. 2007). The coastal plains of the southwest South Island of New Zealand lie within a few tens of kilometres of the Australia–Pacific plate boundary which has ruptured along the Alpine Fault approximately every 329 years for over 8000 years (Berryman et al. 2012). Earthquakes at the southwestern end of the Alpine Fault, where it passes offshore, give rise to a tsunami hazard that may be difficult to identify and quantify, even for historic events (e.g. Goff et al. 2004). Tsunamis commonly contribute to a cascade of seismotectonic hazards along convergent plate boundaries (Atwater 1987; Goff & McFadgen 2002; Patton et al. 2009; Fritz et al. 2012) and may be an agent of substantial erosion, entraining nearshore sand, sometimes to well below wave base (Srinivasalu et al. 2007; Goff et al. 2009).

Major seismic events can also be responsible for rapid geomorphic evolution, due partly to sediment generation during co-seismic landsliding (Goff & McFadgen 2002; Wells & Goff 2006, 2007; Howarth et al. 2012; Robinson & Davies 2013). Post-seismic sedimentary response can be rapid, and in areas that experience intense runoff events the post-earthquake residence time of landslide sediment may be of the order of only a few years (Wang et al. 2015) to decades (Howarth et al. 2012). Together, the sedimentary response, landslide effects, and tsunami generation can drastically alter the landscape by cycles of erosion and accretion of sediment at beaches and other coastal depositional features (Goff et al. 2009). A number of studies have concluded that large Alpine Fault events result in large pulses of sediment (e.g. Berryman et al. 2012; Howarth et al. 2012; Clark et al. 2013) which are efficiently delivered to the catchments during large rainfall events (Fitzsimons et al. 2013). Coastal areas of these catchments record the large rainfall, landslide, and faulting events as pulses of sediments, redistributed by longshore transport and then by wave and wind action to form coastal dunes, are subsequently populated by trees and shrubs within decades of an event (Wells & Goff 2006, 2007).

Wells and Goff (2006) have used tree rings to relate shore-parallel dunes near Haast to major ruptures on the Alpine Fault. They related the youngest dune to the 1826 Fiordland earthquake, which presumably ruptured on the offshore Puysegur section of the Alpine Fault (e.g. Norris & Cooper 2001). Goff et al. (2004) indicate that the tsunami inundation may have extended from Dusky Sound in the south to at least Okarito Lagoon in the north (Figure 1), indicating

CONTACT DC Nobes david.nobes@canterbury.ac.nz
*The authors are not currently affiliated with the University of Canterbury.

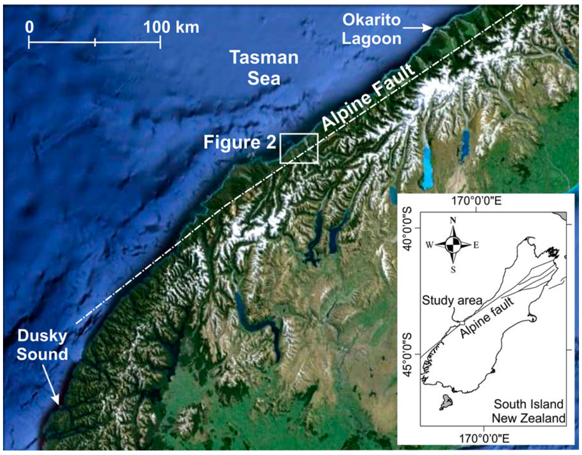

Figure 1. The study site in South Westland, near the Alpine Fault. The 1826 tsunami was observed in Dusky Sound, about 200 km south of our study site, and deposits of that tsunami may have been found in Okarito Lagoon, about 100 km north of our study site. Inset: Location of the study area on the West Coast of the South Island.

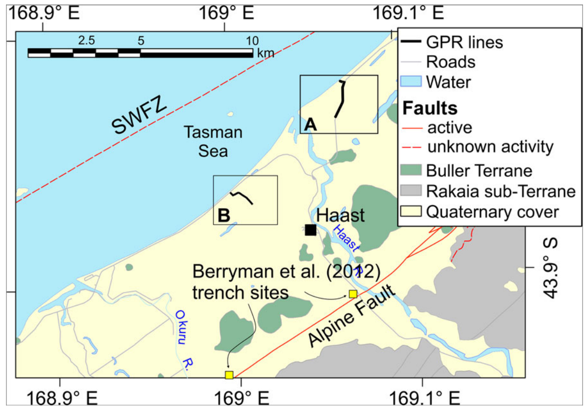

Figure 2. The study location northwest of the Alpine Fault and southeast of the offshore South Westland Fault Zone (SWFZ). **A,** One site was near the mouth of the Haast River, and **B,** a second lay between the Haast River and Okuru River mouths. The Haast profile (A) was acquired in two segments: a shorewards segment running from the highway to the high tide marks; and an inland segment along the side of the highway.

that it may have caused coastal erosion along the Haast coast. While the record is far from certain, we will follow the time-line and dating outlined by Wells and Goff (2006) as a guide to the shore-parallel morphology.

Our initial purpose was to investigate the coastal dune stratigraphy and test whether the observed subsurface stratigraphy fits with the Wells and Goff model of dune formation. Most West Coast sediment pulses incorporate more magnetic sediments (Fitzsimons et al. 2013) which yield good reflections in ground penetrating radar (GPR) profiles (e.g. Meyers et al. 1996; Smith et al. 1999).

We report the results of our analysis of new GPR and complementary electrical imaging (EI) data from two sites in South Westland, near Haast. The radargrams reveal dune sequences building seawards on top of the interpreted wave-base platform and on previously deposited dune sequences. This is what we expected to see and was observed, for example, by Meyers et al. (1996), Smith et al. (1999) and Peterson et al. (2010). In some cases, these could be interpreted as storm event erosional features or retreat scarps (e.g. Meyers et al. 1996; Peterson et al. 2010); in others however, the truncating features extend to the wave base and at two sites appear to disrupt the wave base. Strong storms are not known to disturb or disrupt the wave base. One location was near the Haast River mouth where we observe truncated bedding on the face of the second-youngest coastal dune, and the other was inland, crossing an old access track and coincident with a steeply incised stream channel. The age constraints provided by the dune vegetation suggests that the disruption of the wave-base reflection, which superficially resembles low-angle faulting, is caused either by low-angle slope failure or by tsunami erosion of the dune face, possibly during the elusive 1826 tsunami.

Site description and survey methodology

The Alpine Fault is located less than 10 km to the southeast of the study sites (Figures 1, 2). A second large tectonic feature, the South Westland Fault Zone (SWFZ), lies a similar distance to the northwest of the study area, offshore of Haast (Figure 2). Its activity and recurrence are unknown, but it has been presumed to be inactive in recent times (e.g. Sutherland 1996; Sircombe & Kamp 1998; Rattenbury et al. 2010). The Alpine Fault generates coseismic landslides that provide pulses of sediments to the local catchments (e.g. Howarth et al. 2012; Clark et al. 2013). These sediments are then transported to the Tasman Sea (Figures 1–3) where they are distributed by longshore drift, accreted to the shore face, and form linear shore-parallel beach ridges in the decades immediately following a major Alpine Fault event (Wells & Goff 2006, 2007). By using tree-ring dating, each ridge has been attributed to an Alpine Fault event (Figure 3A).

We investigated two sites: one near the Haast River mouth in South Westland, New Zealand; and a second halfway between the mouths of the Haast River and Okuru River, along an old access track that starts next to the Haast landfill road entrance (Figures 2, 3). We used GPR and electrical imaging methods at the sites along the shorter shorewards line (Figure 3A, short line adjacent to the shore) and GPR alone for the longer profiles along the Haast Highway (Figure 3A) and the Haast landfill road (Figure 3B). The shorewards profile extended northwest towards the sea from the highway, whereas the road profiles extended inland to the south and southeast. Other profiles are not presented here because they were either dominated by

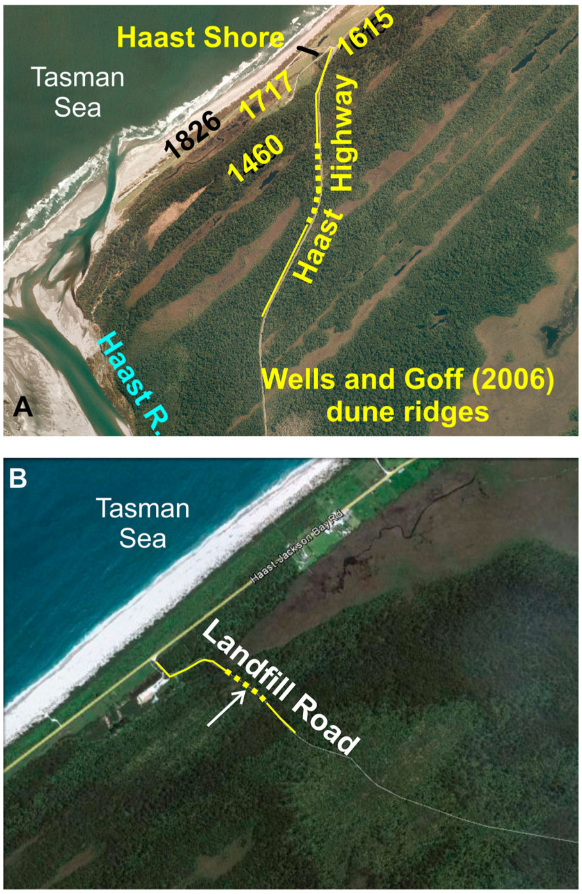

Figure 3. Detailed views of the two survey locations. **A,** The Haast shore and Haast Highway profile locations are northeast of the Haast River mouth. The dune ridge dates from the Wells and Goff (2006) model are shown for reference. The segment of the Haast Highway profile shown in Figure 6 is indicated by the dashed line. **B,** The Haast landfill road profile started next to the highway and then followed an old supply track. The location of the stream cut noted in the text and in Figures 12 and 13 is highlighted by an arrow. The segment of the profile used in Figure 13 is indicated by the dashed line.

recent river erosion and deposition, or were adversely affected by seawater along the shore.

GPR

Ground penetrating radar (GPR) has become a widely used tool in subsurface imaging. The reader is referred to Davis and Annan (1989) and Milsom and Eriksen (2011) for descriptions of how GPR works.

The GPR data were gathered using a Sensors & Software pulse EKKO 100A system, equipped with 50 and 100 MHz antennas. The 50 MHz profiles were acquired by stepping the antennas along the profile at 0.5 m intervals. This was close to the lateral sampling resolution of the antennas, which is equal to the optimal trace spacing. The 100 MHz GPR profiles were acquired with the antennas mounted on a sled which was towed slowly; regularly spaced fiducial markers placed along the line to check the speed allowed for later interpolation to a regular trace spacing. The 100 MHz profiles were generally slightly oversampled, which yields good continuity of reflections and of any subsurface diffractions. Both sets of antennas were used at the Haast River mouth (HRM) site. The depth of penetration of the 100 MHz signal is almost as good as for the 50 MHz signal and the resolution is better, so only the 100 MHz antennas were used for the Haast Highway and Haast landfill road profiles.

In addition to the standard common offset profiles, common mid-point/wide-angle reflection and refraction (CMP/WARR) profiles (Hatton et al. 1986; Davis & Annan 1989) were acquired at the HRM site (Figures 3A, 4A). Reflection hyperbolas are generated in the CMP profiles as the source and receiver antennas are separated in a normal move-out step-wise fashion (Figure 4A). Semblance analysis of the CMP hyperbolas (Hatton et al. 1986) allows us to construct a velocity stratigraphy (Figure 4B). The velocities obtained are consistent with partly saturated to saturated sand and

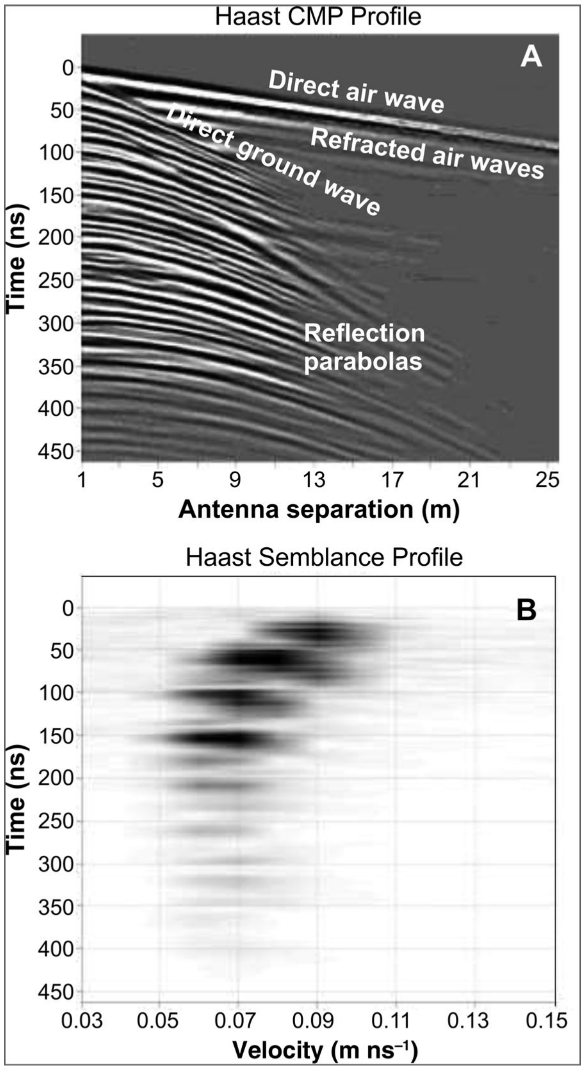

Figure 4. **A,** The Haast CMP profile had no clear direct ground arrival. The air arrival yields a velocity of 0.3 m ns^{-1}, as it should, which calibrates the profile. **B,** The resultant semblance analysis yields velocities that decrease from 0.09 m ns^{-1} (90 m μs^{-1}) in the upper 50 ns to about 0.07 m ns^{-1} (70 m μs^{-1}) below 50 ns.

silt, decreasing from c. 0.09 m ns^{-1} (90 m μs^{-1}) near the surface to c. 0.07 m ns^{-1} (70 m μs^{-1}) at depth. A velocity of 0.07 m ns^{-1} was therefore used for processing the HRM profiles. The few diffractions due to subsurface scattering features present in the Haast profiles are consistent with the semblance analysis velocities. The weather in the days immediately preceding the acquisition of the Haast shore profiles was very wet with widespread flooding; dominance of the water content on the GPR response can affect the GPR velocity. The CMP profiles were gathered on the first dry day.

No CMP/WARR profiles could be gathered at the Haast landfill site because of time and spatial constraints. There were diffractions present however, and the velocities obtained were of the order of 0.1 m ns^{-1} (100 m μs^{-1}), a value more consistent with partly saturated sand. The difference between the Haast shore and Haast landfill road velocities may be due, in part, to the sunny warm weather in the days preceding the acquisition of the Haast landfill profile.

The profiles were further processed using complex attribute analysis (see Kanaswich 1981; Hatton et al. 1986). Each profile is composed of a set of real numbers – traces – that are a record of the antenna voltage as a function of time, $V(t)$. If we take the Hilbert transform of each trace, $\mathcal{H}(V(t))$, we can create a complex number:

$$z(t) = V(t) + i\mathcal{H}(V(t)) = x + iy,$$
$$\text{where } i = \sqrt{-1},$$

which will then have the usual complex attributes of instantaneous amplitude (also called the envelope):

$$|z(t)| = \sqrt{(x^2 + y^2)},$$

instantaneous phase:

$$\phi(t) = tan^{-1}(\mathcal{H}(V(t))/V(t)) = tan^{-1}(y/x),$$

and instantaneous frequency,

$$f(t) = (d\phi/dt)/2\pi.$$

The envelope, or instantaneous amplitude, reflects changes in reflection strength, and is often associated with changes in lithology and sequence boundaries (Taner et al. 1979; Taner 2001). The instantaneous amplitude may therefore be associated with depositional environment changes. Because of reflection strength variations, the instantaneous amplitude may also change at discontinuities such as faults. The instantaneous phase is useful for testing the continuity or connectedness of what are apparently continuous reflections (e.g. Yetton & Nobes 1998). Reflections from bedded sediments can often appear continuous and connected even if they are actually offset in the presence of faulting, particularly if no rotation occurs across the fault. The instantaneous phase helps to identify discontinuities in bedding across, for example, faults and unconformities. The instantaneous frequency is often used as an indicator of textural changes (e.g. Francké & Nobes 2000). As such, it has less of a role here because the textures of dune sediments are similar on both sides of any faults or storm scarps.

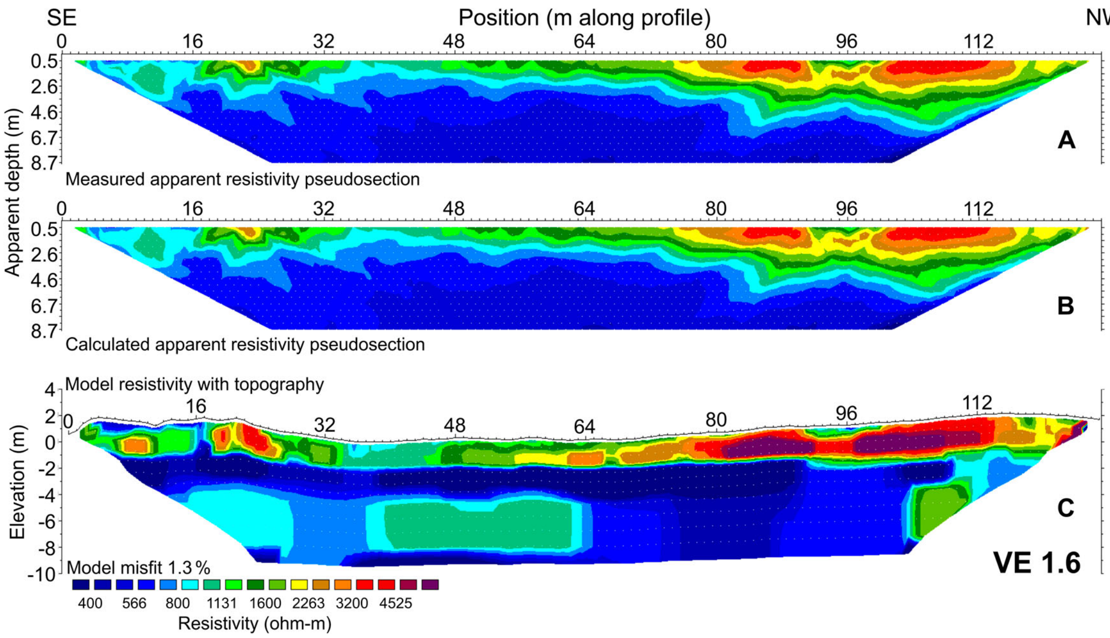

Figure 5. A, The measured apparent electrical resistivity for the HRM EI profile has a **B,** good 'best fit' model response that yields a misfit of only 1.3%. **C,** The 'best-fitting' model including topography has a high-resistivity layer on the top, corresponding to the sand dunes on the surface, and lower-resistivity layers and features at depth below the water table. VE, vertical exaggeration.

Electrical imaging

Electrical imaging (EI) profiles were acquired using a Campus Tigre system with 128 electrodes, deployed at 1 m spacing in a simple Wenner array geometry (e.g. Milsom & Eriksen 2011). The EI profiles were gathered across the youngest coastal dunes near the Haast River mouth (at the shore in Figure 3A). The HRM profile began on the back of the dune that is attributed to the 1717 Alpine Fault earthquake (Figure 3A) and extended 127 m, finishing at the edge of the high tide mark on the beach just north of the HRM.

The data were modelled using the inversion algorithm developed by Loke and Barker (1996) and implemented in the Res2DInv computer modelling and inversion programme. The measured EI response is iteratively modelled until the model converges to a level of 'misfit' that is unchanging; the 'misfit' is the difference between the measured and model responses, expressed as a root-mean squared relative error in percent. Each profile therefore yielded a 'best fit' model that minimised the misfit between the observed apparent resistivities and the model response. Features will be more reliable in the interior of a model than at its edges, because there is less data coverage at the base and at either end of the profile. The models were run with and without topography. The topographically corrected models were then interpreted jointly with the GPR results.

Figure 5 provides an example of a good fit between the measured (Figure 5A) and the modelled responses (Figure 5B) for the HRM EI, with a misfit of only 1.3%. The model which includes topography (Figure 5C) clearly shows the resistive surface layers, especially the highly resistive dunes, and the contrasting more conductive subsurface layers. The electrical images did not extend far enough out onto the tidal shore to record the influence of sea water at depth, but clearly show the contrast between the dunes on the surface above the water table and the deeper strata.

Results

We now consider the profiles moving from north to south, starting with the Haast Highway profile. All profiles have been migrated and corrected for topography. Examples of the sorts of features we expected to see are illustrated in a portion of the Haast Highway GPR profile. The features of interest are difficult to see in the entire profile, so only a small portion is shown here as an example (Figure 6). We observe the GPR reflections from a dune sequence onlapping the seawards slope of a previous dune sequence. The wave base can just be seen at the far left of Figure 6A, at about 350–400 ns two-way travel-time (TWT), or about 12 m below sea level at this location. A possible storm beach can be seen at the top of the dune sequence, at about 400 m along the Haast Highway profile. At about 560 m along the profile, there appear to be truncations of the bedding (arrows in Figure 6), but the truncating feature does not reach the wave base. We interpret this as either a storm beach or possibly a slump feature, given the hummocky character of the material at depth seawards of the arrows.

In contrast, a truncating feature visible across the middle of the Haast shore profiles (Figure 7, highlighted by the dashed line and the arrows) truncates or cross-cuts not only the bedding but also appears to disrupt the wave base at about 300–350 ns TWT or about 8–10 m below current sea level at this location. This would not occur if the linear feature were merely a wave or storm scarp. The slope of the wave base is disrupted and appears to tilt shorewards at a location that coincides with the truncating feature.

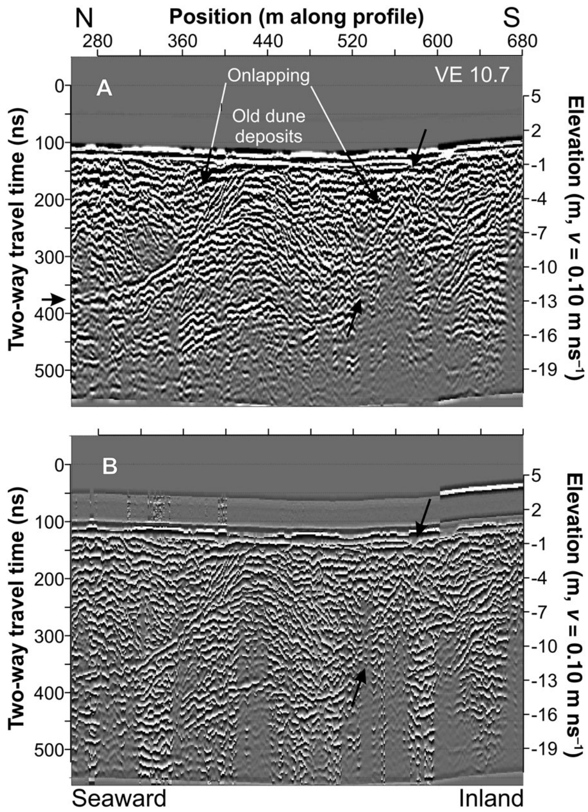

Figure 6. A portion of the **A,** migrated and topographically corrected Haast Highway profile, and **B,** the same section processed for the instantaneous phase, illustrating some characteristic features. The profiles are viewed as if looking from the WSW towards the ENE; the sea is to the north. A dune is visible, centred at about 440 m along the profile. The steepness of the dune face at shallow depths suggests a storm beach front. We see truncated beds at about 560 m along the profile, and some possibly hummocky reflections at depth at about 480 m along the profile to the left of the bottom arrow. This feature could be a storm beach or a slump of sediment triggered by a storm or some other cause. The approximate position of the wave base where it reaches the northern boundary of the profile at the left is indicated with an arrow.

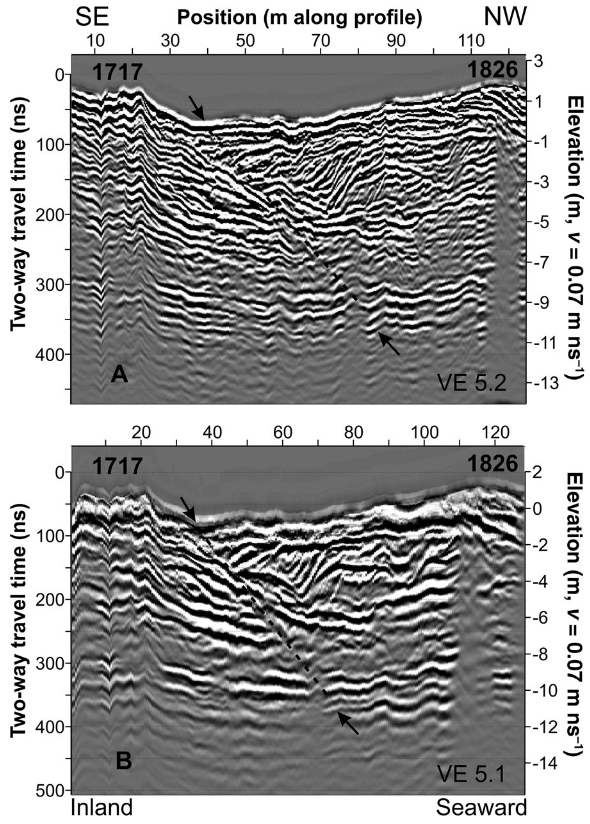

Figure 7. The **A,** 100 MHz, and **B,** 50 MHz HRM profiles appear to have a feature that not only truncates the beds, but also appears to disrupt the wave base at 300–350 ns TWT (about 8–10 m depth) just above the bottom arrows. The feature is clearest in the 50 MHz profile (B). The profiles are approximately SE–NW-aligned. The profiles are viewed as if looking from the NE towards the SW, with the sea to the NW.

The truncating feature is clearest in the 50 MHz profile (Figure 7B). The difference in response is further emphasised by the envelope (Figure 8) and the instantaneous phase (Figure 9), which makes the offsets clearer in the 100 MHz profile (Figures 8A, 9A). It does not appear to be a slump feature, because we do not see hummocky reflections that are characteristic of slumps. The truncating feature is only just visible in the instantaneous frequency profile (Figure 10), which illustrates that the textures across the truncating feature are similar, and the response is dominated by the sandy lithology.

The clear evidence for a truncating and potentially offsetting feature in the GPR data is enhanced by comparing the GPR and EI results (Figure 11), which complement and support each other. The higher resistivity feature (brighter colour) at depth in the EI profiles is truncated by the dipping GPR reflector. Using the migrated and topographically corrected GPR profiles, we estimate the dip of the truncating feature to be about 12–20° to the northwest. The slope looks much steeper in the GPR profiles due to the vertical exaggeration. The mutual agreement of the two datasets then gives us more confidence in each of the individual datasets.

The Haast landfill road (HLR) profile shows both dune-like features in the near surface (Figure 12A) and indications of massive bedding (i.e. lack of reflections, cf. Nobes et al. 2001) both in the near surface (between about 480 and 540 m along the profile) and at depth (at about 120 m along the profile). Closer examination of the HLR profile on either side of the stream channel (Figure 12B) reveals apparent truncations of beds to the northwest (left) of the stream channel. As for the HRM profile, the truncating feature appears to be dipping to the northwest.

Complex attribute analysis of the HLR profile (Figure 13) clarifies the truncating feature, especially in the instantaneous amplitude (Figure 13A), while the lack of continuity of the bed reflections is clearer in the instantaneous phase (Figure 13B). The instantaneous amplitude (Figure 13A) also reveals the presence of another, oppositely dipping, feature to the southeast (right) of the stream channel. The northwest-dipping feature extends to depth and may offset the wave base, although the reflection energy at that depth is not sufficient to be clear. The southeast-dipping feature does not appear to extend much beyond about 4 m in depth but it has significant envelope energy and separates two zones: one with little or no envelope response and another with significant

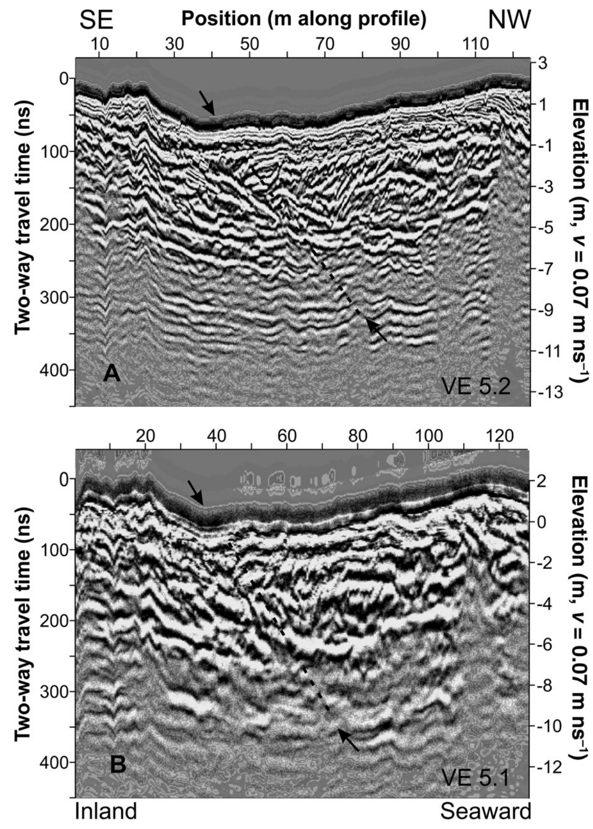

Figure 8. A, The envelope enhances the changes observed across the truncating feature in the 100 MHz HRM profile. The reflections either side of the feature are clearly different. **B,** The changes are not so enhanced in the 50 HRM MHz profile, where the normal GPR profile (Figure 7B) more clearly shows the presence of the truncating feature.

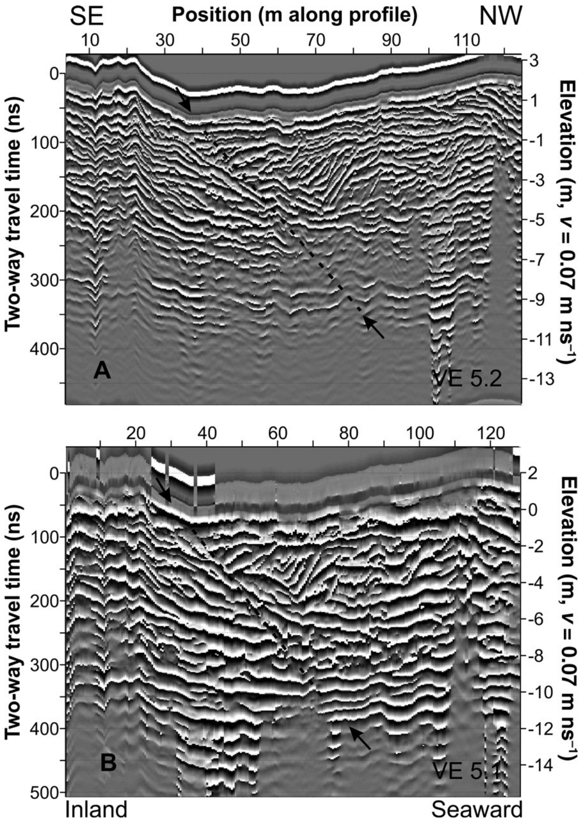

Figure 9. The instantaneous phase profiles corresponding to those in Figures 7 and 8 are shown for the **A,** 100 MHz HRM profile, and **B,** 50 MHz profile. In this case, the linear feature noted in Figures 7 and 8 is more clearly seen in the 100 MHz instantaneous phase (A).

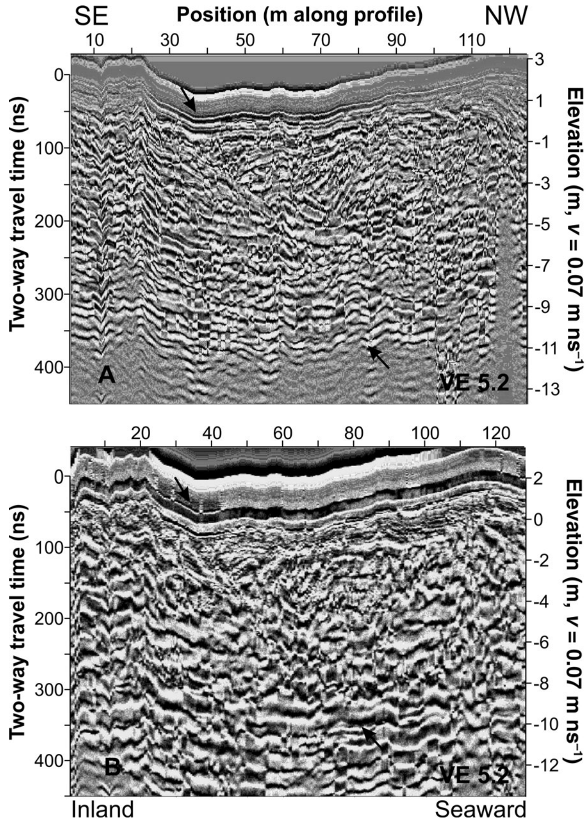

Figure 10. A, The instantaneous frequency shows only minor changes across the possible structure. The differences in the textural response are greater at depth in the 100 MHz HRM profile, below about 60–80 m along the profile. **B,** As for the envelope (Figure 8B) and instantaneous phase (Figure 9B), the instantaneous frequency for the 50 MHz HRM profile does not enhance the response of the truncating feature.

envelope response. Both of the significant dipping features that are clear in the instantaneous amplitude come to the surface at the stream channel.

Discussion

We observe several clear truncations of beds in the geophysical imaging profiles. Bending-moment normal faults can be present in this tectonic context. However, the dips of the truncating features are less than 20°, and are therefore unlikely to be normal faults. The exact angle of a normal fault depends on the friction angle of the material. Dry sand has a friction angle of approximately 30°, so the normal faulting should occur at about 30° to the (vertical) maximum compressive stress. This suggests that a normal fault in sand should be dipping at c. 60°.

Lower-angle failure planes generally require pre-existing structures, high pore pressures, or both. For instance, sliding can occur on low-angle failure planes due to high pore pressures (e.g. Hubbert & Rubey 1959). The anomalous feature could therefore be a lateral-spread feature, with sliding towards a free face on a low-angle slip surface due to co-seismically elevated pore pressures. The shoreline along the South Westland coast drops off steeply, which provides a setting that would be amenable to a slump or a rotational slide. In either case, the event that caused the displacement could be coincident with the earthquake that built the seawards 1826 dune. The beds on either side of the truncating features are difficult to correlate, suggesting that the features are not slip-planes that are offsetting the dune and nearshore stratigraphy. However, difficulty in correlating beds is not the same as a complete lack of correlation. We would also expect to see an indication of a hummocky reflection profile above the wave base if the bed truncations are due to a slip, as we noted in Figure 6 for the Haast Highway profile. The response at depth is not clear enough to distinguish if the beds are hummocky or not. We therefore consider a failure surface to be a possible explanation for these features.

We return then to the 1826 earthquake and the report of a tsunami associated with that event (Goff et al. 2004). The dipping feature in the HRM profile truncates beds that are part of the 1717 dune (Figure 14), which in 1826 would have been the most seawards dune. A tsunami cutface would, in one sense, be an extreme case of a storm-cut beach. As noted earlier, storm-cut beaches are not known to disrupt or displace

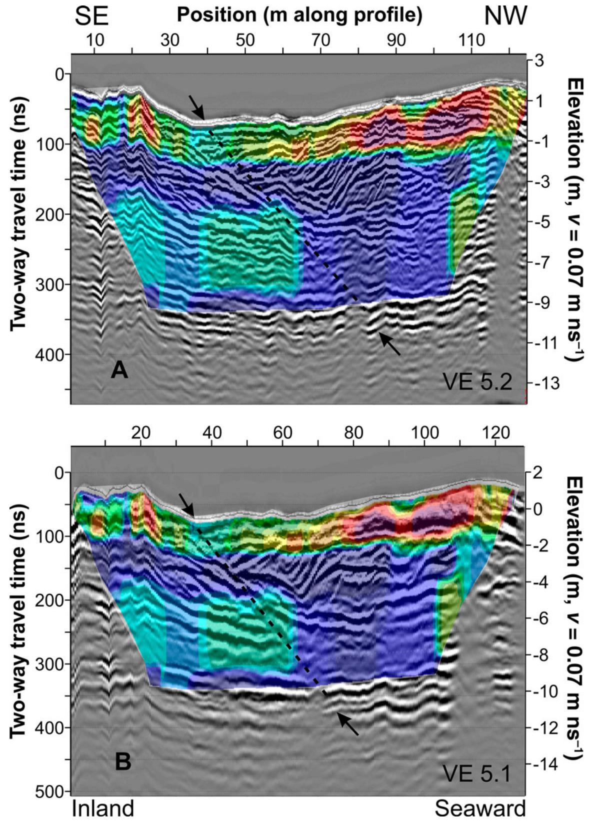

Figure 11. The HRM **A,** GPR 100 MHz and **B,** 50 MHz profiles are shown overlain with the best-fitting resistivity model. A truncating feature is readily apparent and has a clear influence on the subsurface electrical properties as well as on the GPR.

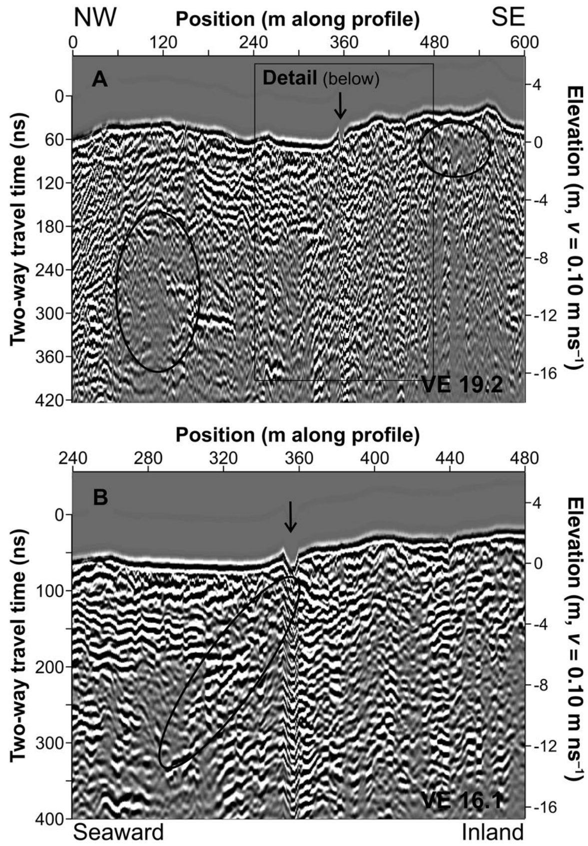

Figure 12. A, The HLR profile, and **B,** a detailed section from 240 to 480 m along the HLR profile highlight near-surface coastal dune features and a possible truncating feature dipping to the northwest, which comes to the surface at an incised stream channel, as indicated by the arrow at about 360 m along the profile. More massive bedding has few or weak reflections (circled in A).

the wave base, but tsunamis have done so. The timing would fit what we observe: the feature truncates the beds of the dune associated with the 1717 Alpine Fault event; the beds on either side do not align, but appear to be independently deposited; the seaward beds build up on the base; and subsequently a coastal dune forms that has been attributed to the 1826 event (Wells & Goff 2007).

The HRM profles can therefore be interpreted as illustrated in Figure 14. The 1717 dune and foreslope deposits (labelled A in Figure 14) were eroded and truncated by a tsunami generated by the 1826 Fiordland event, or were truncated by a co-seismic low-angle failure. The tsunami would hit the 1717 shoreline, causing erosion. Some of the material eroded from A was deposited soon after at the base of the slope (B in Figure 14). There would have been no dune in front of the 1717 dune when the presumed tsunami occurred. Sediments transported alongshore during the aftermath of the 1826 event would be deposited, prograding outwards. The advancing dune would be created at the maximum pulse of sediment and then the swale behind was infilled as or after the foredune had aggraded and became the 'new' shoreline. The unit Bi (Figure 14) represents beds that would have formed as part of the deposition of the new foredune and as deposits infilling the swale that formed behind the new coastal dune. Most of this sediment would have been shoreface deposits filling the 'void' that remained after the tsunami erosion. Continuing cycles of sediment accumulation (C, D, and E in Figure 14) built up the coastal dune deposits, culminating in the foreslope shore accretion (F in Figure 14). Finally, plants became established on the seawards dune (Wells & Goff 2007).

The other similar feature that we observed along the inland HLR profile is suggestive of a similar process, but associated with an earlier event. The deposits lying seawards of the stream cut are truncated by a feature similar to that observed in the HRM profiles. However, the presence of an additional shallowly dipping feature landwards of the stream cut presents the possibility of another tectonic feature controlling the landscape and processes at this site. Given the position of the stream cut the event predates 1717 and possibly 1615, based on the dating of Wells and Goff (2006, 2007). The site is accessible, albeit from a rough track through West Coast temperate rain forest, and future work could determine the exact nature and timing of the event that gave rise to the truncating feature.

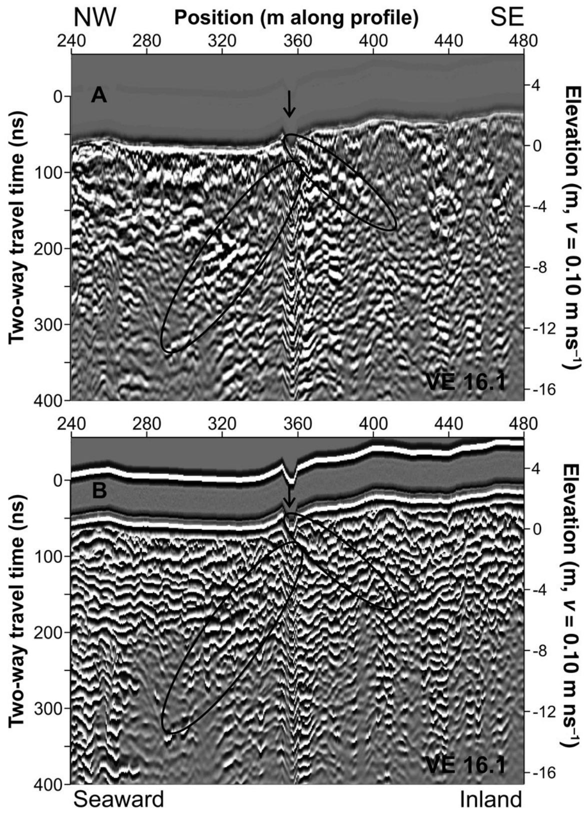

Figure 13. A, The complex attributes envelope, and **B,** instantaneous phase of the subset of the HLR profile shown in Figure 12B enhance the appearance of the truncating feature (circled at depth to the left of the stream) that reaches the surface at the stream cut (arrow). In addition, in the envelope response (B) there also appears to be a feature dipping inland (circled, to the right of the stream) to the southeast away from near the crest of the stream cut.

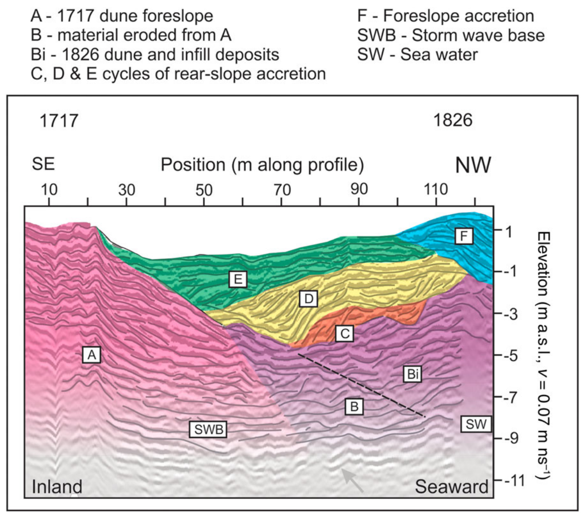

Figure 14. An interpretive diagram incorporating the reflections observed along all of the HRM profiles. **A,** The 1717 dune deposits overlie the storm wave base (SWB), and are truncated by the feature noted in the text and in Figures 10–13. **B,** Some of the material eroded from A was initially deposited at the base of the 1717 dune deposits. **C–E,** The start of the deposition in the aftermath of the 1826 event then built coastal dune and infill deposits (Bi), followed by cycles of sediment accretion. **F,** Finally, the dune foreslope sediments were deposited. Seawater (SW) impedes penetration of the radar signal.

Conclusions

Geophysical imaging of the beach ridges near the mouth of the Haast River reveals the presence of a linear feature that appears to truncate the bedding in the nearshore dunes and to disrupt the wave base, which we would not expect if it were simply a storm scarp. A similar feature is observed to truncate beds along an old access road adjacent to the Haast landfill road, and there is an incised stream channel where this feature comes to surface. The dips are too shallow and the field relationships indicate that the features are too young to be normal faults, so we suggest that the truncations are likely due to erosion either by a shallowly dipping slip triggered by an event on the nearby Alpine Fault or by a tsunami associated with the 1826 Fiordland earthquake. Given how close the structures come to the surface, it may be possible to test our hypotheses by trenching or other similar means.

Acknowledgements

We thank Brittany Charlton, Nick Jaeger and Nick Topper for their invaluable field assistance. They worked tirelessly and well. We thank the reviewers and Professor Andrew Gorman for their constructive comments which helped to improve the manuscript.

Associate Editor: Associate Professor Andrew Gorman.

Disclosure statement

No potential conflict of interest was reported by the authors.

Funding

The project was funded by the University of Wisconsin–Eau Claire International Fellows Program and supported by the Department of Geography and Anthropology, University of Wisconsin-Eau Claire and the Department of Geological Sciences, University of Canterbury.

References

Atwater BF. 1987. Evidence for great Holocene earthquakes along the outer coast of Washington State. Science. 236:942–944.

Berryman KR, Cochran UA, Clark KJ, Biasi GP, Langridge RM, Villamor P. 2012. Major earthquakes occur regularly on an isolated plate boundary. Science. 336:1690–1693.

Clark KJ, Cochran UA, Berryman KR, Biasi G, Langridge R, Villamor P, Bartholomew T, Litchfield N, Pantosti D, Marco S, et al. 2013. Deriving a long paleoseismic record from a shallow-water Holocene basin next to the Alpine Fault, New Zealand. GSA Bull. 125(5/6):811–832.

Davis JL, Annan AP. 1989. Ground penetrating radar for high-resolution of soil and rock stratigraphy. Geophys Prospect. 37:531–551.

Fitzsimons SJ, Howarth JD, Upton P, Koons PO. 2013. High magnitude, low frequency rainfall events drive landscape development in the Southern Alps. In: Reid CM, Wandres A, editors. Abstracts, Geosciences 2013

Conference, Christchurch, New Zealand. Geoscience Society of New Zealand Miscellaneous Publication 136A; p. 32.
Francké J, Nobes DC. 2000. A preliminary evaluation of GPR for nickel laterite exploration. In: Noon DA, Stickley GF, Longstaff D, editors. GPR 2000: Proceedings of the 8th International Conference on Ground Penetrating Radar. Society of Photo-Optical Instrumentation Engineers (SPIE). 4084:7–12.
Fritz HM, Phillips DA, Okayasu A, Shimozono T, Liu H, Mohammed F, Skanavis V, Synolakis CE, Takahashi T. 2012. The 2011 Japan tsunami current velocity measurements from survivor videos at Kesennuma Bay using LiDAR. Geophys Res Lett. 39(7):L00G23.
Goff JR, Lane E, Arnold J. 2009. The tsunami geomorphology of coastal dunes. Nat Hazards Earth Syst Sc. 9:847–854. doi:10.5194/nhess-9-847-2009.
Goff JR, McFadgen BG. 2002. Seismic driving of nationwide changes in geomorphology and prehistoric settlement—a 15th century New Zealand example. Quat Sci Rev. 21(20–22):2229–2236.
Goff JR, Wells A, Chagué-Goff C, Nichol SL, Devoy RJN. 2004. The elusive AD 1826 tsunami, South Westland, New Zealand. NZ Geogr. 60(2):28–39.
Hatton L, Worthingon MH, Makin J. 1986. Seismic data processing: theory and practice. Oxford: Blackwell Scientific Publications.
Howarth JD, Fitzsimons SJ, Norris RJ, Jacobsen GE. 2012. Lake sediments record cycles of sediment flux driven by large earthquakes on the Alpine Fault, New Zealand. Geology. 40(12):1091–1094.
Hubbert MK, Rubey WW. 1959. Role of fluid pressure in the mechanics of overthrust faulting. Bull Geol Soc Am. 70:115–205.
Kanaswich ER. 1981. Time sequence analysis in geophysics. 3rd ed. Edmonton: University of Alberta Press. 483 p.
Loke MH, Barker RD. 1996. Rapid least-squares inversion of apparent resistivity pseudosections by a quasi-Newton method. Geophys Prospect. 44:131–152.
Meyers RA, Smith DG, Jol HM, Peterson CD. 1996. Evidence for eight great earthquake-subsidence events detected with ground-penetrating radar, Willapa barrier, Washington. Geology. 24:99–102.
Milsom J, Eriksen A. 2011. Field geophysics. 4th ed. Chichester: Wiley & Sons.
Nobes DC, Ferguson RJ, Brierley GJ. 2001. Ground-penetrating radar and sedimentological analysis of Holocene floodplains: insight from the Tuross valley, New South Wales. Aust J Earth Sci. 48:347–355.
Norris RJ, Cooper AF. 2001. Late Quaternary slip rates and slip partitioning on the Alpine Fault. NZ J Struct Geol. 23:507–520. doi:10.1016/S0191-8141(00)00122-X.
Patton JR, Goldfinger C, Morey A, Erhardt M, Black B, Garrett A, Djadjadihardja Y, Hanifa U. 2009. 7.5 KA earthquake recurrence history in the region of the 2004 Sumatra-Andaman earthquake. GSA Annual Meeting, Paper No. 154–8.
Peterson CD, Jol HM, Vanderbergh S, Phipps JB, Percy D, Gelfenbaum G. 2010. Dating of late Holocene beach shoreline positions by regional correlation of coseismic retreat events in the Columbia Rover littoral cell, USA. Mar Geol. 273:44–61.
Quigley MC, Sandiford M, Cupper ML. 2007. Distinguishing tectonic from climatic controls on range-front sedimentation. Basin Res. 19(4):491–505.
Rattenbury MS, Jongens R, Cox SC. 2010. Geology of the Haast area. Institute of Geological and Nuclear Sciences 1:250 000. Geological Map 14. Lower Hutt: GNS Science.
Robinson TR, Davies TRH. 2013. Potential geomorphic consequences of a future great (Mw = 8.0+) Alpine Fault earthquake, South Island, New Zealand. Nat Hazards Earth Syst Sci. 13:2279–2299.
Sircombe KN, Kamp PJJ. 1998. The South Westland Basin: seismic stratigraphy, basin geometry and evolution of a foreland basin within the Southern Alps collision zone, New Zealand. Tectonophysics. 300(1–4):359–387.
Smith DG, Meyers RA, Jol HM. 1999. Sedimentology of an upper-mesotidal (3.7 m) Holocene barrier, Willapa Bay, SW Washington, USA. J Sediment Res. 69(6):1290–1296.
Srinivasalu S, Thangaduraia N, Switzerb AD, Mohanc VR, Ayyamperumal T. 2007. Erosion and sedimentation in Kalpakkam (N Tamil Nadu, India) from the 26th December 2004 tsunami. Mar Geol. 240:65–75. doi:10.1016/j.margeo.2007.02.003.
Sutherland R. 1996. Transpressional development of the Australia-Pacific boundary through southern South Island, New Zealand: Constraints from Miocene-Pliocene sediments, Waiho-1 borehole, South Westland. New Zeal J Geol Geophys. 39(2):251–264.
Taner MT. 2001. Seismic attributes. CSEG Recorder. 26 (7):48–56.
Taner MT, Koehler F, Sheriff RE. 1979. Complex seismic trace analysis. Geophysics. 44:1041–1063.
Wang J, Jin Z, Hilton RG, Zhang F, Densmore AL, Li G, West AJ. 2015. Controls on fluvial evacuation of sediment from earthquake-triggered landslides. Geology. 43:115–118.
Wells A, Goff J. 2006. Coastal dune ridge systems are chronological markers of palaeoseismic activity: a 650-yr record from southwest New Zealand. The Holocene. 16 (4):543–550.
Wells A, Goff J. 2007. Coastal dunes in Westland, New Zealand, provide a record of paleoseismic activity on the Alpine Fault. Geology. 35(8):731–734.
Yetton MD, Nobes DC. 1998. Recent vertical offset and near-surface structure of the Alpine Fault in Westland, New Zealand, from ground penetrating radar profiling. New Zeal J Geol Geophys. 41:485–492.